Available online at www.sciencedirect.com
ScienceDirect
Geochimica et Cosmochimica Acta 74 (2010) 3260–3273
Geochimica et Cosmochimica Acta
www.elsevier.com/locate/gca

Synthetic fluid inclusions XVIII: Experimental determination of the PVTX properties of H_2O–CH_4 to 500 °C, 3 kbar and X_{CH4} ⩽4 mol.%

Fang Lin, R.J. Bodnar *

Fluids Research Laboratory, Department of Geosciences, Virginia Tech, Blacksburg, VA 24061, USA

Received 30 June 2009; accepted in revised form 9 March 2010; available online 16 March 2010

Abstract

The pressure–volume–temperature–composition (PVTX) properties of H_2O–CH_4 were determined from the bubble point curve to 500 °C and 3 kbar for compositions ⩽4 mol.% CH_4 using the synthetic fluid inclusion technique. H_2O–CH_4 inclusions were produced by loading known amounts of Al_3C_4 and H_2O into platinum capsules along with pre-fractured and inclusion-free quartz cores. During heating the Al_3C_4 and H_2O react to produce CH_4, and the H_2O–CH_4 homogeneous mixture was trapped as inclusions during fracture healing at elevated temperature and pressure. The composition of the fluid in the inclusion was confirmed using the weight loss technique after the experiment and by Raman spectroscopic analysis of the inclusions.

Homogenization temperatures of the inclusions were determined and the results were used to construct iso-T_h lines, defined as a line connecting the formation temperature and pressure with the homogenization temperature and pressure. The pressure in the inclusion at the homogenization temperature was calculated from the Duan equation of state (EOS). The slope ($\Delta P/\Delta T$) of each iso-T_h line was calculated and the results fitted to a polynomial equation using step-wise multiple regression analysis to estimate the slope of the iso-T_h line as a function of the homogenization temperature and composition according to:

$$(\Delta P/\Delta T) = a + b \cdot m + c \cdot m^4 + d \cdot (T_h)^2 + e \cdot m \cdot T_h + f \cdot m \cdot (T_h)^4,$$

where $\Delta P/\Delta T$ is the slope of the iso-T_h line in bars/°C, m is the CH_4 molality, T_h is the homogenization temperature in degrees Celsius, and a, b, c, d, e, f are the fitting parameters. The equation is valid from the bubble point curve to 500 °C and 3 kbar for compositions ⩽4 mol.% CH_4.

1. INTRODUCTION

Methane (CH_4)-bearing aqueous fluids have been reported from a number of geologic settings, including sedimentary basins (Pironon et al., 2003; Dubessy et al., 2001; Hao et al., 1998), low-grade (Mullis et al., 1994; Vityk et al., 1996) to high-grade (Hall and Bodnar, 1990) metamorphic terrains, mid-ocean ridge hydrothermal systems (Kelley, 1996), ore-forming systems (Hall et al., 1991), and anthracite coalfields (Kisch and Van den Kerkhof, 1991). Many CH_4-bearing aqueous fluids that occur in the earth's crust are adequately modeled by the binary H_2O–CH_4 system (Dubessy et al., 2001). Addition of CH_4 to aqueous solutions affects both the phase equilibrium and volumetric properties of the solution, and failure to recognize the presence of small amounts of methane can cause significant errors in pressures estimated from fluid inclusions (Hanor, 1980; Roedder and Bodnar, 1980; Roedder, 1984).

Over the past half-century, many workers have investigated the phase equilibrium properties of H_2O–CH_4 at

* Corresponding author. Tel.: +1 540 231 7455; fax: +1 540 231 3386.
E-mail address: rjb@vt.edu (R.J. Bodnar).

0016-7037/$ - see front matter © 2010 Elsevier Ltd. All rights reserved.
doi:10.1016/j.gca.2010.03.009

various pressure-temperature-composition (PTX) conditions. Culberson and McKetta (1951), Price (1979) and Ashmyan et al. (1985) reported experimental data on solubility of CH_4 in water. Krader and Franck (1986) determined the high temperature boundary between the one-phase (liquid or vapor) and two-phase (liquid plus vapor) fields for two compositions in the H_2O–CH_4 system, and Jacobs and Kerrick (1981), Saxena and Fei (1988) and Zhang et al. (2007) developed thermodynamically-based equations of state for the H_2O–CH_4 system. However, there are relatively few experimental studies of the volumetric (PVTX) properties of H_2O–CH_4 at elevated temperatures and pressures. Welsh (1973) studied the H_2O–CH_4 system to 200 °C and 10 kbar for compositions between 4 and 85 mol.% CH_4. Zhang and Frantz (1992) studied compositions between 5.5 and 16.5 mol.% CH_4 at 400 to 600 °C and 1-3 kbar. The present study focuses on the lower concentration range (0-4 mol.% CH_4) at moderate temperature and pressure. Such conditions are relevant to sedimentary basins and low-grade metamorphic environments in which the fluids contain only a few mol.% CH_4 (Mullis et al., 1994; Guillaume et al., 2003).

2. EXPERIMENTAL METHODS

2.1. Starting materials and sample preparation

Synthetic H_2O–CH_4 fluid inclusions were produced using the synthetic fluid inclusion technique introduced by Sterner and Bodnar (1984) and Bodnar and Sterner (1987), with minor modifications as described below. Quartz cores approximately 4 mm in diameter and 5-10 mm long or 2 mm × 3 mm × 5 mm quartz prisms were cut from inclusion-free Brazilian quartz. The quartz cores and prisms were cleaned by first soaking in 30% H_2O_2 solution, followed by 2 M HNO_3 solution and finally boiling in doubly-distilled H_2O to remove organic, heavy metal and other contaminants that may have been introduced to the surface of the quartz cores and prisms during cutting. After cleaning, the quartz cores and prisms were heated to 350 °C for 3–4 h. The quartz cores and prisms were removed from the oven and immediately dropped into cool doubly distilled H_2O. The thermal shock produced numerous microfractures in the quartz cores and prisms, and these serve as the sites of inclusion formation as the fractures heal during later hydrothermal experiments. After fracturing, the quartz was placed into a vacuum oven overnight at approximately 125 °C to remove any water that might have entered the fractures during the fracturing event.

Hydrothermal experiments to trap H_2O–CH_4 inclusions were conducted in cold-seal pressure vessels. Platinum capsules containing the starting materials were prepared in the following manner. First, a known amount of aluminum carbide (Al_4C_3), 20–30 mg fused silica glass powder, a fractured quartz core or prism, and a known amount of distilled and deionized water were loaded into a platinum capsule (~5 mm i.d. and 25–35 mm long). Silica glass powder was added to enhance the solubility of SiO_2 in the solution to promote fracture healing. Aluminum carbide served as the source of CH_4, based upon the following reaction:

$$Al_4C_3 + 12H_2O = 3CH_4 + 4Al(OH)_3. \quad (1)$$

The amounts of Al_4C_3 and H_2O required were determined based on the desired final CH_4 concentration and were calculated using the reaction stoichiometry in Eq. (1). After all components were loaded, the capsule was sealed with a Pt end cap using arc welding.

After cleaning and weighing, sealed Pt capsules containing known initial weights of H_2O and Al_4C_3 were placed into horizontally mounted cold-seal hydrothermal vessels to trap synthetic fluid inclusions. The synthetic fluid inclusions were formed at 300–700 °C and 1, 3 and 5 kbar to assure trapping conditions in the single-fluid-phase field. Pressure was monitored using a Bourdon-type Heise gauge and is considered to be accurate to within 50–100 bars. Temperatures, measured using chromel–alumel thermocouples, are accurate to ±3 °C. The capsules were quenched at the end of the run (ranging from about 5 days for 700 °C experiments to 40 days for 300 °C experiments) by removing the vessels from the furnaces and allowing them to cool to room temperature. The capsules were removed from the pressure vessels, cleaned to remove any residue from the surface, dried and weighed. Capsules with equal weights before and after the run were assumed to have not leaked and were processed for analysis.

The fluid composition in the capsule at the completion of the experiment (and, presumably, in the fluid inclusions) was confirmed by comparing the fluid composition in the capsule at the end of the run to the expected composition based on the amount of water and aluminum carbide originally loaded into the capsule and based on the reaction stoichiometry given by Eq. (1). The fluid composition in the capsule at the completion of the run was determined in the following manner, modified from that of Schmidt and Bodnar (2000). The cleaned capsule was wrapped with 8-fold Kimwipe tissue paper and placed into a small glass vial. A sharpened stainless steel needle was also placed in the glass vial. The weight of the entire assembly, consisting of glass vial + tissue + capsule + needle was recorded at room temperature. Next, the Pt capsule was carefully punctured by pushing the needle through the tissue and into the platinum capsule. A hissing sound was heard when the capsule was punctured and gas escaped. The tissue around the needle trapped any solid material that escaped from the capsule during puncturing, and absorbed the small amount of liquid water that was expelled from the capsule with the gas. Immediately after puncturing the capsule, the entire assembly was weighed again. The weight loss recorded at this stage represents CH_4 gas lost from the capsule as a result of opening. The potential effect of oxidation of CH_4 to CO_2 during the experiment is discussed in the next section. The amount of CH_4 remaining in the capsule dissolved in the water at room temperature and pressure is negligible, considering the solubility of CH_4 in water at 25 °C and 1 bar is only about 20 ppm (cf. Duan et al., 1992c). After determining the amount of gas loss, the assembly was placed into a vacuum oven and heated at 120 °C to evaporate the water that was absorbed by the tissue and water

that remained in the capsule after piercing. After approximately 5–10 h, the assembly was removed from the oven, cooled to room temperature, and weighed again. The difference in weight between this step and that measured immediately after piercing represents the mass of the H_2O in the capsule, assuming that $Al(OH)_3$ remains stable and does not transform into Al_2O_3 during heating – an issue that is discussed in the next section. We found that the Kimwipe tissue devolatilizes during heating and contributes a small amount (usually 0.005–0.02 g) to the weight difference attributed to H_2O. Therefore, a control assembly, consisting of glass vial + tissue + needle, was placed in the oven together with each batch of capsules. The weight loss experienced by the control assembly was subtracted from the weight loss for the experimental capsules to determine the mass of H_2O in the capsule during the experiment (and after puncturing). The composition of the H_2O–CH_4 fluid inclusion was then calculated from the measured weights of CH_4 and H_2O in the capsule. If the composition determined by weight loss did not agree within experimental error (±0.3 mol.% CH_4) with the composition based on the amounts of components originally loaded into the capsule, the sample was discarded. If the composition calculated from the amount of aluminum carbide and water originally loaded into the capsule (based on the reaction stoichiometry indicated by (1)) and post-run weight loss measurements agreed, the quartz core was processed in preparation for microthermometric analysis. A comparison of the measured and predicted compositions for the samples used for PVTX determinations is shown in Fig. 1. It is worth noting that the experimental error associated with sample weighing is small compared to the total mass of CH_4 in the capsules. For example, the precision of the balance used is ±5 μg, while the amount of methane in the capsules ranged from 200 to 800 μg.

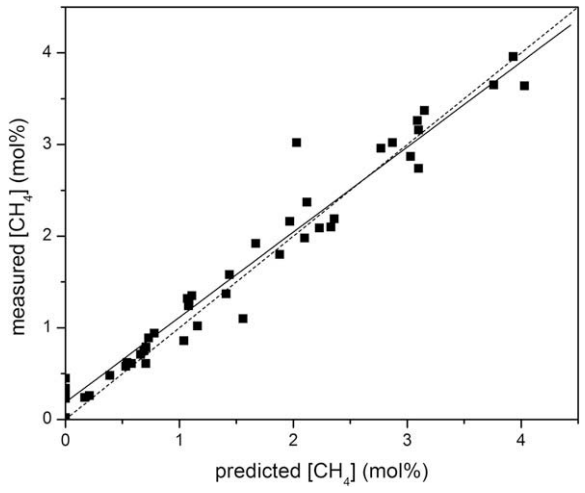

Fig. 1. Comparison of the predicted CH_4 concentration in the capsules with that measured by weight loss at the completion of the inclusion synthesis experiment. The dash line represents a perfect 1:1 correlation. The solid line represents a linear fit line to the experimental data.

Two issues related to the use of aluminum carbide as the source of methane for high temperature experiments were identified during the course of this study. The first concerns the freshness of the aluminum carbide. Al_4C_3 undergoes photochemical decomposition when exposed to light, and slowly decomposes when exposed to moisture at room temperature. The initial calibration experiments for this study used aluminum carbide from a bottle that had been opened and used previously in another study. The amounts of CH_4 generated by the Al_4C_3–H_2O reaction were about 1/3 of the predicted amounts (Fig. 2a–c), and the measured and predicted CH_4 concentrations differed by ≈60–70% (Fig. 2d). In contrast, a second calibration experiment conducted under the same condition (150 °C, 1 atm. external pressure) as the previous experiment but using a new batch of Al_4C_3 that had been sealed under argon by the manufacturer (Sigma–Aldrich Inc.), generated essentially identical measured and predicted compositions (Fig. 2e–g). The difference in measured and predicted compositions agreed within 12% for concentrations between 3 and 5 mol.%, and within 5% for CH_4 concentrations lower than 3 mol.% (Fig. 2h). Based on these results, all of the samples used in this study were prepared with aluminum carbide taken from containers immediately after breaking the manufacturer's seal and loaded directly into platinum capsules. After each capsule loading event (usually involving 10–20 capsules) the remaining aluminum carbide was discarded and a new bottle used for each subsequent batch of capsules.

The second issue related to the aluminum carbide starting material concerns the reaction stoichiometry. Chou et al. (2001) used Al_3C_4 to generate CH_4 gas in their experiments, but they described the reaction of aluminum carbide with water as:

$$Al_4C_3 + 6H_2O = 3CH_4 + 2Al_2O_3. \quad (2)$$

Initially, the reaction stoichiometry suggested by Chou et al. (2001) was used to determine our predicted methane concentration, but this did not produce satisfactory results. In an attempt to identify the cause of this discrepancy we conducted X-ray powder diffraction analysis of the reaction products from experiments conducted at 150 °C and 1 atm. The results confirmed that the solid remaining in the capsule after the reaction of aluminum carbide with water is $Al(OH)_3$ and not Al_2O_3 (Fig. 3). Other workers have shown that aluminum hydroxides can dehydrate into aluminum oxides at elevated temperatures (Paglia, 2004). However, those studies were conducted under dry "melt" conditions, i.e., the aluminum hydroxide was heated in the absence of an aqueous phase.

Comparison of CH_4 concentrations calculated using the two different reaction stoichiometries shows that the difference in calculated CH_4 concentration is small for compositions less than about 4 mol.% CH_4 (Fig. 4), which is the upper composition limit for this study. However, uncertainties in the reaction stoichiometry can lead to significant errors for CH_4 concentrations higher than 4 mol.%. It should also be noted that the study of Chou et al. (2001) did not require a known or controlled CH_4

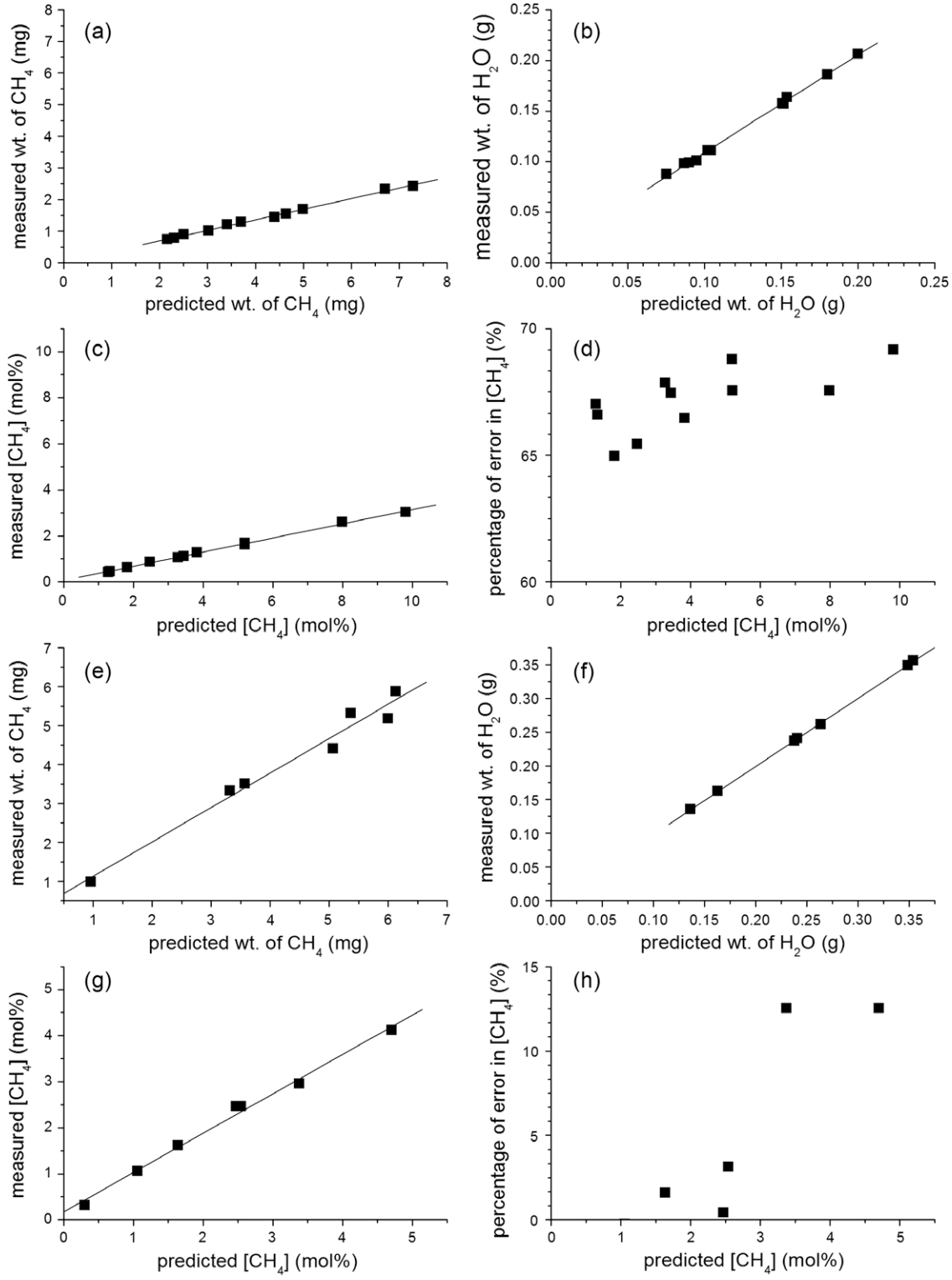

Fig. 2. Comparison of the predicted versus measured CH_4 and H_2O weight and the CH_4 concentration produced using older (a–c) and fresh (e–g) Al_3C_4 to generate CH_4. The percent errors in CH_4 concentration for the experiment using the old and using the fresh Al_3C_4 are shown in figures d and h, respectively. Both sets of experiments were conducted at 150 °C, 1 atm external pressure. The solid lines are the trend lines fit to the data by linear regression.

concentration – the only requirement was that the analytical volume contained both water and methane. Thus, the uncertainty in reaction stoichiometry should not affect their results.

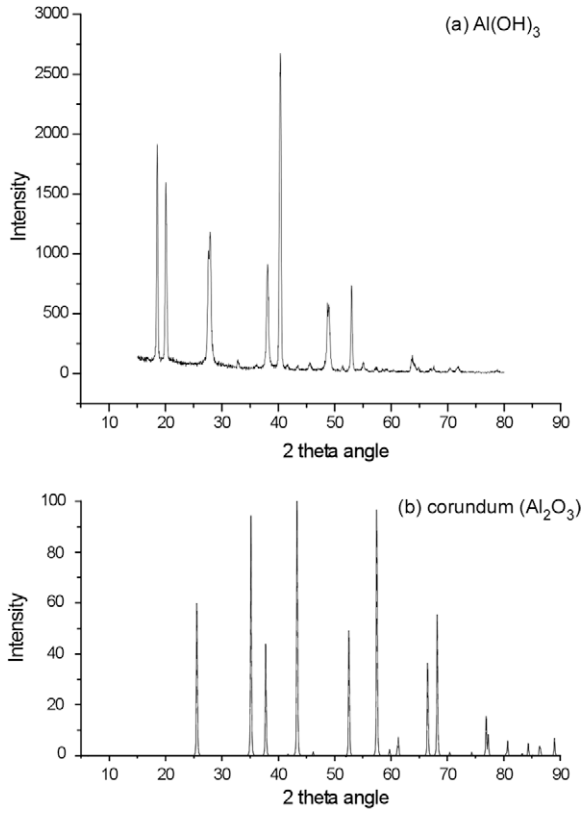

Fig. 3. X-ray powder diffraction pattern of the solid material remaining in the capsule at the end of an experiment (top) and the spectrum of a natural corundum crystal for comparison (bottom). The residual was collected from experiment 092203 conducted at 150 °C, 1 atm external pressure. The analysis was conducted using a Scintag X-ray powder diffractometer with CuKα radiation (1.54 Å wavelength). The diffraction pattern of the residual material after the experiment confirms that the solid material is $Al(OH)_3$.

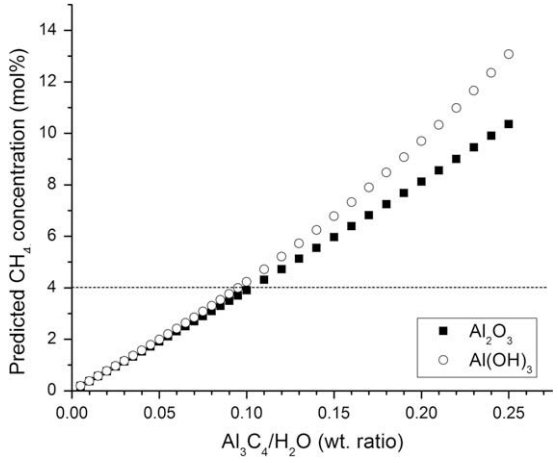

Fig. 4. Comparison of the effect of assumed reaction stoichiometry on the predicted composition of H_2O–CH_4 fluids generated by the Al_3C_4–H_2O reaction. In this study, all compositions studied contained $\leqslant$4 mol.% CH_4 (horizontal dashed line).

2.2. Effect of formation conditions on fluid composition

Depending on the oxidation state and the temperature and pressure, CH_4 may react with H_2O to produce CO_2 and H_2 (Zhang and Frantz, 1992; Murphy and Roberts, 1997; Lamb et al., 2002) according to the following reaction:

$$CH_4 + 2H_2O = CO_2 + 4H_2. \quad (3)$$

At elevated temperatures, the amount of CO_2 generated through the above reaction can be promoted through diffusion of H_2 out of Pt capsules. Some workers have taken steps to minimize this problem, such as using thick-wall gold capsules (Zhang and Frantz, 1992; Lamb et al., 1996, 2002), and/or using Ar or CH_4 gas as the pressure medium to increase the hydrogen fugacity in the cold-seal pressure vessel (Lamb et al., 1996, 2002). In this study, the samples were run in platinum capsules, water was used as the pressure medium, and the pressure vessels were constructed from high-Ni alloy (René 41). Thus, in our experiments the conditions in the pressure vessels were more oxidizing than in the experiments of Zhang and Frantz (1992) and Lamb et al (1996, 2002) and were more likely to generate CO_2.

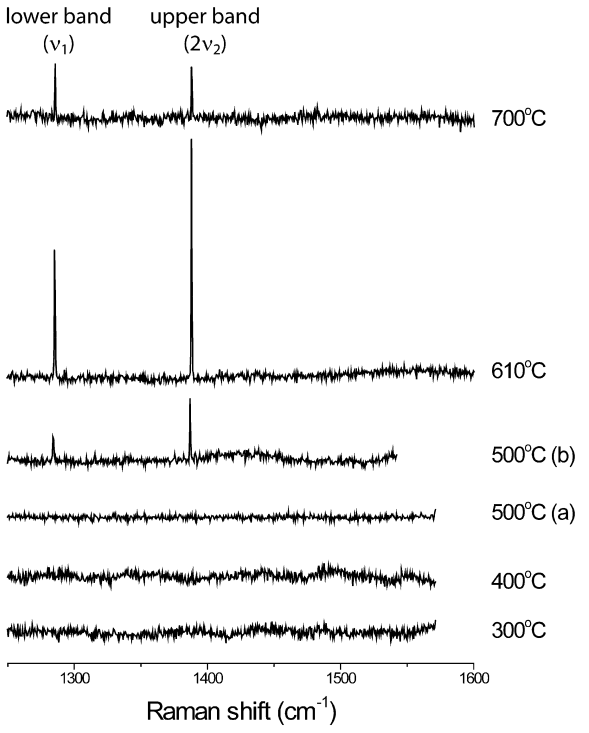

Fig. 5. Raman spectra of synthetic fluid inclusions trapped at various temperatures from 300 to 700 °C. The Fermi diad of CO_2 at 1285 cm^{-1} and 1388 cm^{-1} confirms the presence of carbon dioxide in the inclusions. Carbon dioxide was not detected in inclusions trapped at 300, 400 or in the 500 °C samples containing <5 mol.% CH_4 (spectrum labeled "500 °C (a)"), but was found in inclusions trapped at 500 °C and containing >5 mol.% CH_4 (spectrum labeled "500 °C (b)") and in the inclusions formed at 610 and 700 °C.

Table 1
Formation conditions and microthermometric data for the synthetic inclusions.

Sample ID	T_f (°C)[a]	P_f (bar)[b]	(CH_4) (mol.%)[c]	Mean T_h (°C)[d]	Range (°C)[e]	N[f]	SD[g]
091504-1	500	1000	0	357.9	3.3	30	0.78
091504-2	500	1000	0.39	356.4	1.3	37	0.30
091504-3	500	1000	0.73	358.8	1.0	23	0.20
091504-4	500	1000	1.41	359.0	1.1	25	0.34
091504-5	500	1000	1.88	358.7	1.5	27	0.43
091504-6	500	1000	2.77	360.1	1.5	24	0.37
091504-7	500	1000	3.76	361.4	1.7	25	0.43
092604-1	500	2000	0	305.0	3.7	32	0.86
092604-2	500	2000	0.17	305.4	0.8	27	0.23
022704-1	500	2000	0.21	307.3	1.9	31	0.72
092604-4	500	2000	0.69	308.7	2.7	26	0.63
092604-3	500	2000	0.71	308.0	2.5	27	0.55
022704-2	500	2000	0.78	309.9	2.7	30	0.90
092604-5	500	2000	1.67	312.8	1.3	27	0.34
092604-6	500	2000	2.33	315.9	2.7	30	0.46
092604-7	500	2000	2.87	319.8	3.8	33	0.77
111004-1	500	3000	0	262.6	3.1	36	0.69
111004-3	500	3000	0.71	270.1	3.1	31	0.75
111004-4	500	3000	1.07	270.6	4.6	31	0.99
111004-2	500	3000	2.23	281.5	4.5	40	1.28
111004-5	500	3000	3.09	289.6	3.4	25	0.79
070705-7	400	1000	0	304.3	7.3	12	2.61
070705-8	400	1000	0.53	305.2	8.9	18	2.49
070705-10	400	1000	1.16	309.8	11.0	17	3.55
070705-12	400	1000	3.1	323.2	9.0	14	2.87
040405-5	400	1000	3.93	326.9	4.2	15	1.25
052605-1	400	2000	0	251	9.7	14	3.00
052605-2	400	2000	1.09	260.9	7.6	13	2.37
052605-3	400	2000	2.1	273.2	6.3	8	2.66
052605-4	400	2000	3.1	284.3	8.7	12	3.33
052605-5	400	2000	4.03	291.5	7.8	10	2.64
053005-1	400	3000	0	205.1	4.8	12	1.52
053005-2	400	3000	0.54	216.9	7.5	14	2.31
053005-3	400	3000	1.04	228	8.1	11	2.80
053005-4	400	3000	2.12	250.7	5.7	7	2.11
053005-5	400	3000	3.03	266	6.7	14	2.24
102104-1	300	1000	0	230.2	3.1	15	0.93
102104-2	300	1000	0.66	239.4	9.9	14	2.85
102104-3	300	1000	1.11	246.5	11.8	8	4.66
102104-4	300	1000	1.44	256.4	17.1	5	6.90
102104-5	300	1000	1.97	271.6	12.1	5	4.66
102104-6	300	1000	3.15	281.9	13.9	8	4.06
121004-11	300	2000	0	180.5	3.1	17	0.85
121004-3	300	2000	1.56	227.7	12.1	9	4.51
121004-8	300	2000	2.36	249.3	13.5	10	5.42
070605-1	300	3000	0	141.9	6.4	7	2.05
070605-2	300	3000	0.58	162.5	10.7	10	3.95
070605-3	300	3000	1.08	191.3	9.0	8	3.06
070605-4	300	3000	2.03	227.8	9.6	8	3.70

[a] Formation temperature (°C).
[b] Formation pressure (bar).
[c] Composition (mol.% CH_4).
[d] Arithmetic mean of the measured homogenization temperatures (°C).
[e] Range of the measured homogenization temperatures (°C).
[f] Number of inclusions analyzed.
[g] Standard deviation of the measured homogenization temperatures.

All samples from this study were analyzed by Raman spectroscopy to confirm the presence of CH_4 and to look for evidence of other volatiles. During the analyses, CO_2 was detected in all fluid inclusions trapped at and above 600 °C (Fig. 5). For fluid inclusions trapped at 500 °C, CO_2 was only detected in inclusions containing greater than 5 mol.% CH_4 (Fig. 5). Based on previous work in this laboratory (Rosso and Bodnar, 1995), the detection limit for CO_2 in fluid inclusions is less than 1 bar, and the detection limit of a gas species in a fluid inclusion is determined by the partial pressure of the species in the inclusion, and not its bulk concentration (Wopenka and Pasteris, 1987). Note, however, that inclusion size and depth in the sample, microscope objective, laser power, etc. also affect the detection limits for species in inclusions (Adar et al., 2004). As the total pressure in most inclusions from this study is in the range of several tens to hundreds of bars, the partial pressure (and concentration) of CO_2 is thought to be insignificant in all inclusions trapped at $\leqslant$500 °C. No CO_2 was detected in fluid inclusions trapped at 300 and 400 °C (Fig. 5), and no relationship was observed between the presence of CO_2 and the trapping pressure of the inclusions. A significantly greater mass of gas (compared to the predicted mass assuming only CH_4) was released from those capsules containing samples that later showed CO_2 in the inclusions, similar to observations by Lamb et al. (2002).

According to Eq. (3), hydrogen gas is also generated by the reaction to produce CO_2. However, H_2 gas was not detected in any of the inclusions synthesized in this study. This is not surprising as hydrogen diffuses easily through platinum at elevated temperatures (Chou, 1986), and H_2 is easily lost from fluid inclusions during modest heating (i.e., at heating temperatures above 400–600 °C, Mavrogenes and Bodnar, 1994).

Chou et al. (2008) reported that H_2O and CH_4 can react to produce methanol + hydrogen during heating, as evidenced by Raman peaks for methanol at about 2832 and 2940 cm^{-1}. During Raman screening, no evidence for methanol was found in the inclusions synthesized in this study. We note that Chou et al. (2008) conducted their experiments in fused silica capillaries, which are permeable to hydrogen and therefore promotes the hydrogen-producing reaction (i.e., formation of methanol). Shang et al. (2009) also reported that the diffusion coefficient of hydrogen in fused capillaries at 296 K is about an order of magnitude higher than that of platinum at 723 K (our experimental temperatures were 573–773 K). This may explain why methanol was detected in the experiments of Chou et al. (2008) but not in ours.

2.3. Microthermometric analysis

Samples containing synthetic H_2O–CH_4 inclusions were placed into a FLUID INC-adapted USGS gas-flow heating/cooling stage for microthermometry analysis. The thermocouple was calibrated at 0.0 and 374.1 °C using synthetic fluid inclusions containing pure water, and the reported homogenization temperatures are accurate to within ±1 °C (Sterner and Bodnar, 1984). Homogenization temperatures (denoted as T_h hereafter) of 5–37 inclusions were measured in each sample, each representing a unique P–T–X formation condition. Fewer measurable inclusions ($\geqslant$5 μm) were found in samples formed at lower temperatures (300 °C) compared to samples run at higher temperature. Inclusions of different size and shape and from different locations within the sample were analyzed. Only those samples that showed consistent T_h data were included in the final dataset (see Table 1).

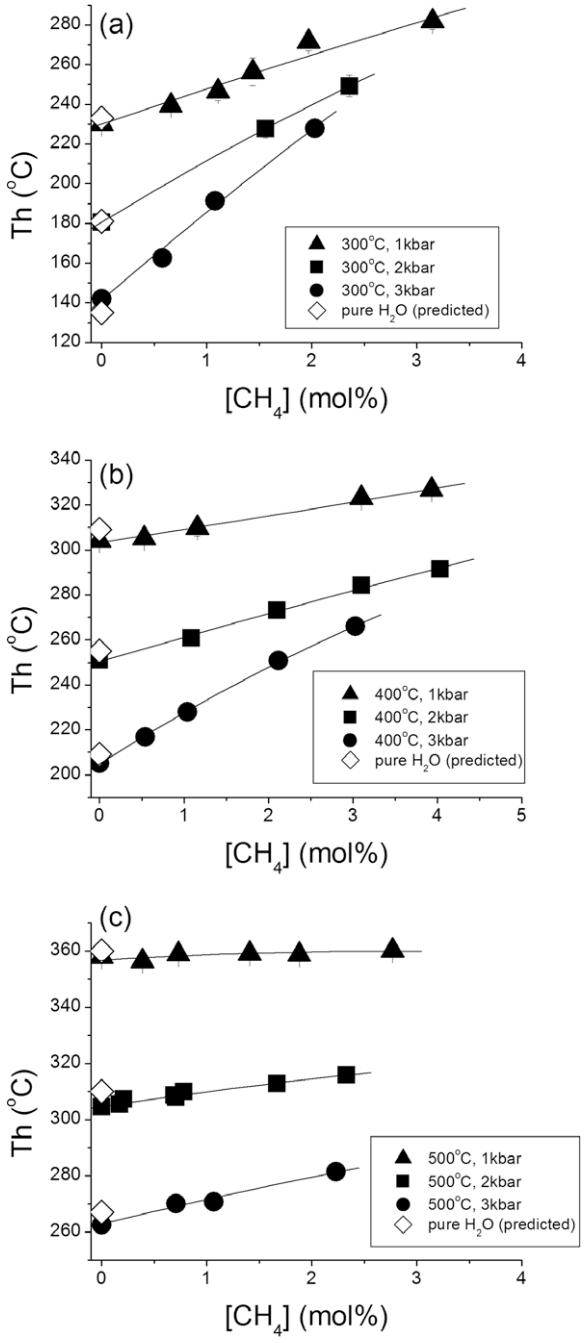

Fig. 6. Relationship between homogenization temperature (T_h) and CH_4 concentration for inclusions trapped at 300 °C (a), 400 °C (b) and 500 °C (c) and pressures of 1–3 kbar. Error bars represent the standard deviation of the T_h values for that sample. In each sample, between 5 and 37 inclusions were measured.

Table 2
Volumetric properties of fluids and slope of iso-T_h lines (isochores).

Sample ID	T_f (°C)[a]	P_f (bars)[b]	T_h (°C)[c]	P_{Th} (bars)[d]	m (CH_4) (molality)[e]	V (cm^3/mol)[f]	V_{EX} (cm^3/mol)[g]	$\Delta V_{Th \rightarrow Tf}$ (%)[h]	$\Delta P/\Delta T$[i]
091504-1	500	1000	357.9	184	0	34.1	0	0.71	5.8
091504-2	500	1000	356.4	194	0.22	–	–	0.72	5.6
091504-3	500	1000	358.8	210	0.41	–	–	0.71	5.6
091504-4	500	1000	359	235	0.79	–	–	0.72	5.4
091504-5	500	1000	358.7	253	1.06	50.4	15.2	0.73	5.3
091504-6	500	1000	360.1	288	1.58	50.9	15.2	0.74	5.1
091504-7	500	1000	361.4	327	2.17	50.4	14.2	0.74	4.9
092604-1	500	2000	305	92	0	26.1	0	0.54	9.8
092604-2	500	2000	305.4	109	0.09	–	–	0.55	9.7
022704-1	500	2000	307.3	115	0.12	–	–	0.54	9.8
092604-4	500	2000	308.7	163	0.39	–	–	0.55	9.6
092604-3	500	2000	308	164	0.39	–	–	0.55	9.6
022704-2	500	2000	309.9	172	0.44	–	–	0.54	9.6
092604-5	500	2000	312.8	267	0.94	32.8	6.2	0.56	9.3
092604-6	500	2000	315.9	340	1.32	32.1	5.2	0.57	9.0
092604-7	500	2000	319.8	395	1.64	31.3	4.3	0.57	8.9
111004-1	500	3000	262.6	49	0	23.3	0	0.38	12.4
111004-3	500	3000	270.1	174	0.40	30.8	7.2	0.38	12.3
111004-4	500	3000	270.6	247	0.60	27.3	3.7	0.40	12.0
111004-2	500	3000	281.5	488	1.27	26.0	2.1	0.43	11.5
111004-5	500	3000	289.6	673	1.77	26.6	2.8	0.45	11.1
070705-7	400	1000	304.3	92	0	26.0	0	0.22	9.5
070705-8	400	1000	305.2	145	0.30	–	–	0.23	9.0
070705-10	400	1000	309.8	212	0.65	33.9	7.3	0.23	8.7
070705-12	400	1000	323.2	410	1.78	33.4	5.7	0.23	7.7
040405-5	400	1000	326.9	498	2.27	32.3	4.2	0.24	6.9
052605-1	400	2000	251	41	0	22.7	0	0.13	13.2
052605-2	400	2000	260.9	275	0.61	26.3	3.2	0.16	12.4
052605-3	400	2000	273.2	512	1.19	25.8	2.3	0.18	11.7
052605-4	400	2000	284.3	752	1.77	25.8	2.1	0.20	10.8
052605-5	400	2000	291.5	1048	2.33	26.0	1.9	0.26	8.8
053005-1	400	3000	205.1	17	0	21.1	0	0.05	15.3
053005-2	400	3000	216.9	207	0.30	23.3	2.0	0.05	15.3
053005-3	400	3000	228	399	0.58	22.6	1.2	0.05	15.1
053005-4	400	3000	250.7	795	1.20	22.9	1.2	0.06	14.8
053005-5	400	3000	266	1130	1.73	23.0	1.1	0.09	14.0
102104-1	300	1000	230.2	28	0	21.9	0	0.04	13.9
102104-2	300	1000	239.4	204	0.37	25.9	3.6	0.05	13.1
102104-3	300	1000	246.5	334	0.62	24.6	2.2	0.05	12.5
102104-4	300	1000	256.4	402	0.81	24.9	2.3	0.03	13.7
102104-5	300	1000	271.6	482	1.12	25.1	2.2	−0.03	18.2
102104-6	300	1000	281.9	815	1.80	24.8	1.4	0.03	10.2
121004-11	300	2000	180.5	10	0	20.4	0	−0.03	16.7
121004-3	300	2000	227.7	752	0.88	22.1	1.3	−0.03	17.3
121004-8	300	2000	249.3	1019	1.34	22.1	1.0	−0.05	19.4
070605-1	300	3000	141.9	4	0	19.4	0	−0.13	19.0
070605-2	300	3000	162.5	468	0.32	20.0	0.5	−0.09	18.4
070605-3	300	3000	191.3	830	0.61	19.9	0.3	−0.12	20.0
070605-4	300	3000	227.8	1333	1.15	20.1	0.2	−0.14	23.1

note: The dash bars "–" for V and V_{EX} of some samples means that those parameters are not calculated for the samples, because of large uncertainties associated with the pressure determination of those samples at room temperature ($P < 10$ bars at room temperature).

[a] Formation temperature (°C).
[b] Formation pressure (bars).
[c] Arithmetic mean of the measured homogenization temperatures (°C).
[d] Pressure (bars) on the liquid vapor curve at the measured homogenization temperature, the pressure was calculated using the equation of Duan et al. (1992b).
[e] Composition (CH_4 molality).
[f] Molar volume at temperature of homogenization (cm^3/mol).
[g] Excess volume at formation temperature and pressure (cm^3/mol).
[h] The volume change (percent) of the inclusion from the formation conditions to the homogenization conditions.
[i] Slope of the iso-T_h line (bars/°C).

3. RESULTS AND DISCUSSION

All inclusions produced in this study contained two phases (an aqueous liquid phase and a CH_4-rich gas phase) when observed at room temperature. The single exception is sample 070605-1, formed at 300 °C and 3 kbar and containing pure H_2O, which contained metastable 1-phase liquid inclusions together with the more common two phase (liquid plus vapor) inclusions. Such single-phase, metastable inclusions are common in samples formed at high pressure, low temperature conditions (Roedder, 1971; Invernizzi et al., 1998). Upon heating, all the 2-phase inclusions from all samples homogenized into the liquid aqueous phase, indicating that all the fluid inclusions trapped a single liquid phase at formation conditions.

The mean T_h of fluid inclusions from each sample increases systematically with increasing CH_4 concentrations (Fig. 6). The relationship between mean T_h and CH_4 concentration is adequately described by second order polynomial equations for experiments run at 300, 400 and 500 °C. Pure H_2O samples generated T_h values equivalent (±3 °C) to those predicted from the water steam tables (Haar et al., 1984) as was observed previously by Bodnar and Sterner (1985).

The goal of this study was to produce internally consistent experimental data that could be used to interpret microthermometric results from fluid inclusions containing low concentrations (⩽4 mol.%) of CH_4. When fluid inclusions are trapped in the one-phase field, it is necessary to know the temperature of homogenization, the pressure inside the inclusion at homogenization, and the slope of the isochore in P–T space, in order to estimate a pressure correction and determine a trapping temperature (Roedder and Bodnar, 1980). Isochores represent lines of constant density or volume and, to a first approximation, fluid inclusions represent isochoric systems. However, owing to the small change in volume due to thermal expansion and compressibility of the host mineral, fluid inclusions are not truly isochoric (see Bodnar and Sterner, 1985; Sterner and Bodnar, 1991). For this reason, many fluid inclusion workers use iso-T_h lines as these more accurately reflect the P–T paths that fluid inclusions follow in P–T space (Bodnar and Vityk, 1994; Bodnar, 1995; Schmidt et al., 1995; Bodnar, 2003a). The deviation of each iso-T_h line from a constant volume (isochoric) path is listed in Table 2.

A straight line connecting the temperature and pressure of formation of the inclusion and the temperature and pressure at homogenization represents an iso-T_h line. The temperature and pressure of formation are known for each inclusion from the experimental conditions, and the homogenization temperature is known from microthermometric analysis of the inclusions, requiring only the pressure inside the inclusion at homogenization to calculate the iso-T_h line. All of the inclusions in this study homogenize along the bubble point curve separating the two-phase (liquid plus vapor) field from the single-phase liquid field. While the pressure in the inclusion at the moment of homogenization cannot be measured directly, it can be calculated from the known homogenization temperature and fluid composition using an appropriate equation of state. Phase boundaries for 0, 0.5, 1, 2, 3, and 4 mol.% CH_4 compositions, calculated from the equation of state of Duan et al.

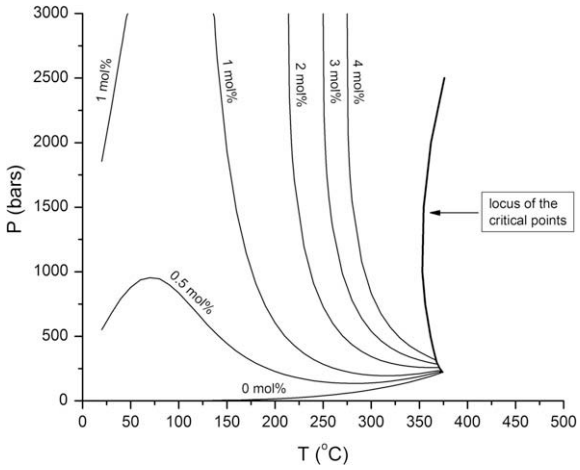

Fig. 7. Two-phase (liquid plus vapor) boundaries of H_2O–CH_4 fluids labeled in mol.% CH_4. At temperatures higher than those on the isopleths (or at pressures higher than those on the isopleths) a single phase H_2O–CH_4 fluid with the indicated composition is stable, whereas two fluid phases coexist at lower temperatures and/or pressures. The phase boundaries were calculated using the Duan et al. (1992a) equation of state. Data for the locus of critical points are from Welsh (1973).

Table 3
Fitting parameters for Eq. (4). The standard error for each fitting coefficient is shown in parentheses.

Fitting coefficients	
a	19.53860 (0.87515)
b	30.49833 (5.81374)
c	−1.859E−2 (0.01086)
d	−1.0733E−4 (1.046E-5)
e	−1.2478E−1 (2.512E−2)
f	8.56213E−10 (2.03428E−10)

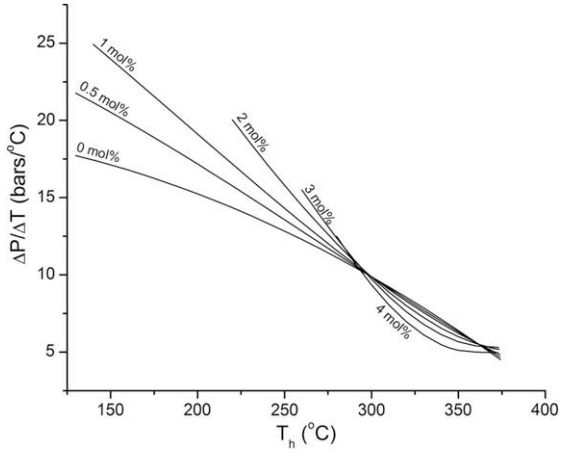

Fig. 8. The slopes of iso-T_h lines ($\Delta P/\Delta T$) in bars/°C as a function of homogenization temperature (T_h) calculated from Eq. (4).

(1992b), are shown in Fig. 7. The EOS of Duan et al. (1992b) was used to calculate the pressure in the fluid inclusions at homogenization.

The slope ($\Delta P/\Delta T$) of the iso-T_h line was calculated for each of the 49 samples in this study. The results are listed in Table 2. The data were analyzed using a step-wise multiple regression algorithm to determine a relationship between the slope of the iso-T_h lines and the composition and homogenization temperature according to:

$$(\Delta P/\Delta T) = a + b \cdot m + c \cdot m^4 + d \cdot (T_h)^2 + e \cdot m \cdot T_h + f \cdot m \cdot (T_h)^4, \quad (4)$$

where $\Delta P/\Delta$T is the slope of the iso-T_h line in bars/°C, m is the CH_4 molality, T_h is the homogenization temperature in degrees Celsius, and a, b, c, d, e, f are the fitting parameters (Table 3). The mean square error (MSE) of the regression analysis is 1.392 with an R^2 value of the fitted equation of 0.9153. The standard error of each fitting coefficient is listed in Table 3. The equation is valid from the bubble point curve up to 500 °C and 3 kbar for compositions $\leqslant$4 mol.% CH_4.

The slopes (ΔP/ΔT) of iso-T_h lines as a function of homogenization temperature and composition for 0, 0.5, 1, 2, 3, and 4 mol.% CH_4 calculated using Eq. (4) are shown in Fig. 8. The slopes of all iso-T_h lines decrease with increasing temperature, as expected. Note that at low temperatures (<300 °C) the slopes of CH_4-bearing compositions are steeper than that of pure H_2O (i.e., the CH_4-bearing fluids are less compressible than H_2O). At higher temperatures the

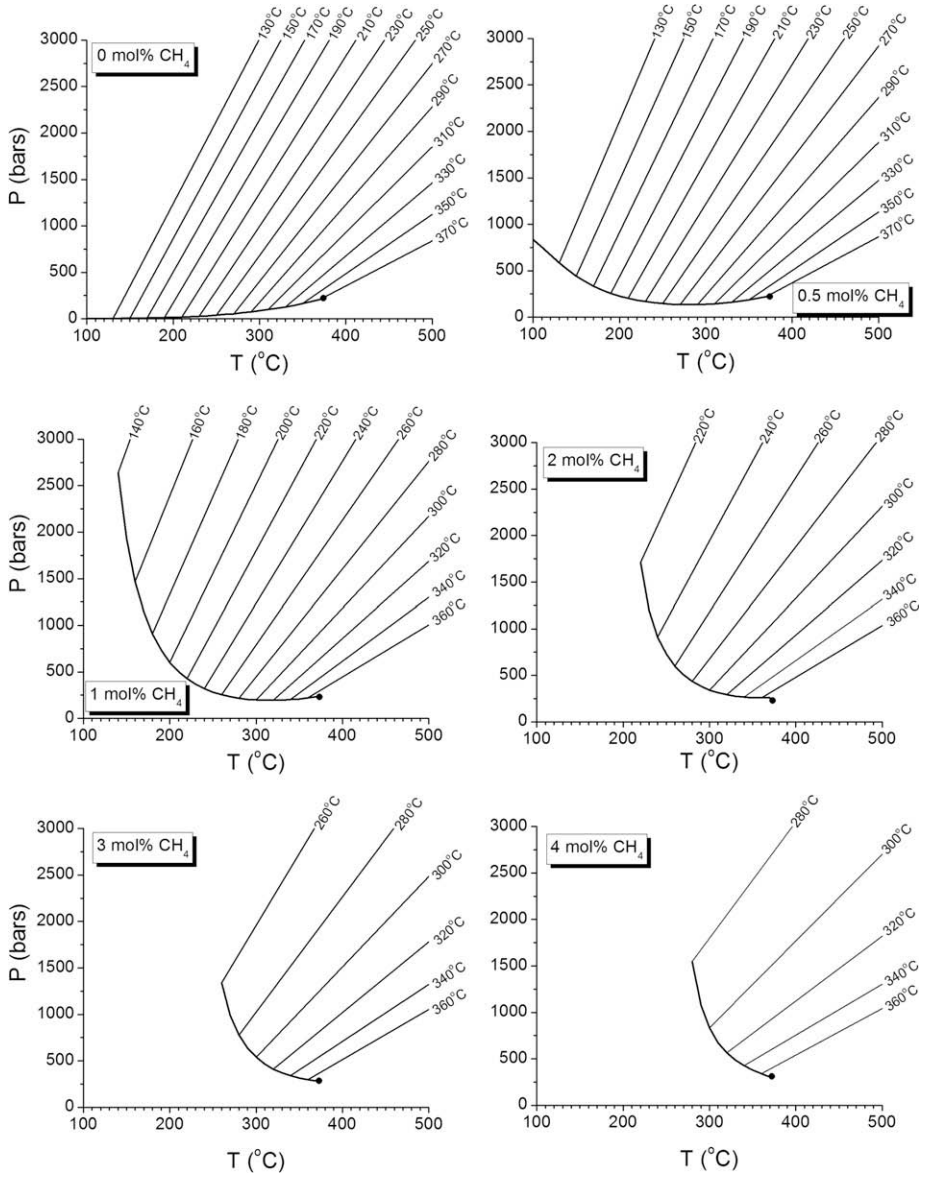

Fig. 9. Iso-T_h lines for 0, 0.5, 1, 2, 3, and 4 mol.% H_2O–CH_4 fluids estimated from the experimental data from this study. The bold lines are liquid-vapor boundaries (see Fig. 7) and the black dots at the high temperature end of the liquid-vapor curves represent the critical point for that fluid composition. The iso-T_h lines are labeled with the appropriate homogenization temperature.

Table 4
Comparison of volumetric data from this study with published values.

Sample ID	T_f (°C)[a]	P_f (bars)[b]	T_h (°C)[c]	P_{Th} (bars)[d]	m (CH_4) (molality)[e]	This study		Model results[*]	
						V (cm^3/mol)[f]	ρ_{Th} (g/cm^3)[g]	V (cm^3/mol)[f]	ρ_{Th} (g/cm^3)[g]
091504-1	500	1000	357.9	184	0	34.1		34.1	0.053
091504-2	500	1000	356.4	194	0.22	–		33.2	0.543
091504-3	500	1000	358.8	210	0.41	–		33.9	0.530
091504-4	500	1000	359	235	0.79	–		34.1	0.527
091504-5	500	1000	358.7	253	1.06	50.4	0.359	34.2	0.526
091504-6	500	1000	360.1	288	1.58	50.9	0.355	34.4	0.522
091504-7	500	1000	361.4	327	2.17	50.4	0.358	34.4	0.521
092604-1	500	2000	305	92	0	26.1		26.0	0.692
092604-2	500	2000	305.4	109	0.09	–		25.8	0.699
022704-1	500	2000	307.3	115	0.12	–		26.0	0.694
092604-4	500	2000	308.7	163	0.39	–		26.3	0.685
092604-3	500	2000	308	164	0.39	–		26.2	0.687
022704-2	500	2000	309.9	172	0.44	–		26.4	0.681
092604-5	500	2000	312.8	267	0.94	32.8	0.551	27.0	0.667
092604-6	500	2000	315.9	340	1.32	32.1	0.563	27.5	0.654
092604-7	500	2000	319.8	395	1.64	31.3	0.576	28.0	0.640
111004-1	500	3000	262.6	49	0	23.3		23.3	0.773
111004-3	500	3000	270.1	174	0.40	30.8	0.587	23.6	0.762
111004-4	500	3000	270.6	247	0.60	27.3	0.661	23.7	0.761
111004-2	500	3000	281.5	488	1.27	26.0	0.693	24.1	0.745
111004-5	500	3000	289.6	673	1.77	26.6	0.679	24.4	0.735
070705-7	400	1000	304.3	92	0	26.0		26.0	0.693
070705-8	400	1000	305.2	145	0.30	–		25.9	0.695
070705-10	400	1000	309.8	212	0.65	33.9	0.531	26.5	0.678
070705-12	400	1000	323.2	410	1.78	33.4	0.538	28.5	0.629
040405-5	400	1000	326.9	498	2.27	32.3	0.556	29.2	0.615
052605-1	400	2000	251	41	0	22.7		22.7	0.793
052605-2	400	2000	260.9	275	0.61	26.3	0.685	23.2	0.777
052605-3	400	2000	273.2	512	1.19	25.8	0.698	23.6	0.762
052605-4	400	2000	284.3	752	1.77	25.8	0.696	23.9	0.752
052605-5	400	2000	291.5	1048	2.33	26.0	0.692	23.9	0.751
053005-1	400	3000	205.1	17	0	21.1		21.2	0.852
053005-2	400	3000	216.9	207	0.30	23.3	0.773	21.3	0.844
053005-3	400	3000	228	399	0.58	22.6	0.795	21.6	0.832
053005-4	400	3000	250.7	795	1.20	22.9	0.785	22.4	0.804
053005-5	400	3000	266	1130	1.73	23.0	0.781	22.4	0.800
102104-1	300	1000	230.2	28	0	21.9		21.9	0.823
102104-2	300	1000	239.4	204	0.37	25.9	0.696	22.2	0.812
102104-3	300	1000	246.5	334	0.62	24.6	0.731	22.4	0.803
102104-4	300	1000	256.4	402	0.81	24.9	0.722	22.9	0.785
102104-5	300	1000	271.6	482	1.12	25.1	0.716	23.5	0.763
102104-6	300	1000	281.9	815	1.80	24.8	0.723	23.6	0.760
121004-11	300	2000	180.5	10	0	20.4		20.4	0.883
121004-3	300	2000	227.7	752	0.88	22.1	0.812	21.3	0.843
121004-8	300	2000	249.3	1019	1.34	22.1	0.813	22.0	0.819
070605-1	300	3000	141.9	4	0	19.4		19.4	0.928
070605-2	300	3000	162.5	468	0.32	20.0	0.899	19.7	0.914
070605-3	300	3000	191.3	830	0.61	19.9	0.903	20.1	0.894
070605-4	300	3000	227.8	1333	1.15	20.1	0.894	20.8	0.863

[a] Formation temperature (°C).
[b] Formation pressure (bars).
[c] Arithmetic mean of the measured homogenization temperatures (°C).
[d] Pressure (bars) on the liquid vapor curve at the measured homogenization temperature, the pressure was calculated using the equation of Duan et al. (1992b).
[e] Composition (CH_4 molality).
[f] Molar volume at temperature of homogenization (cm^3/mol).
[g] Density of water–methane fluid at at formation temperature and pressure (g/cm^3).
[*] Calculated using EOS of Duan and Mao, 2006 (http://geochem-model.org/fluidinc/h2o_ch4/calc.php).

CH_4-bearing fluids are slightly more compressible than H_2O (slopes are less steep). The lowest T_h value shown for each composition corresponds to either 125 °C or the temperature corresponding to a pressure of 3 kbar on the bubble point curve for that composition.

Using Eq. (4), iso-T_h lines have been calculated in increments of 20 °C for six compositions between 0 and 4 mol.% CH_4 and the results are plotted in Fig. 9. The highest temperature and pressure of the experiments is 500 °C and 3 kbar, and these empirical iso-T_h lines should be extrapolated beyond these limits with caution. It should be noted that the pressures along the bubble-point curve shown in Fig. 9 extend to >1 kbar for several of the compositions. In practice, many fluid inclusions in quartz will stretch or decrepitate if the internal pressure exceeds about 1 kbar during heating (Bodnar et al., 1989; Bodnar, 2003b).

Molar volumes of H_2O–CH_4 were calculated using a mass balance technique similar to that used by Sterner and Bodnar (1991) for H_2O–CO_2. At room temperature (22 °C), the pressure in the CH_4 vapor bubble was determined based on the position of the CH_4 Raman peak using the calibration of Lin et al. (2007). Pressures determined by this method were compared with those predicted by Eq. (3) of Lu et al. (2007). The pressure values determined by the two methods differ less than 5 bars in all the cases. After determining the pressure in the inclusion at 22 °C, the solubility of methane in H_2O at 22 °C and at this calculated pressure, and the aqueous phase density at these same conditions, were determined using the EOS of Duan and Mao (2006). The density of the vapor phase (assumed to be pure CH_4) was obtained from Lemmon et al. (2005). Finally, using the known bulk composition combined with the calculated compositions of the liquid and vapor phases, and the densities of the liquid and vapor phases, the bulk density of the inclusion was determined using mass balance constraints. Then, the bulk density was converted to molar volume at 22 °C and the pressure in the inclusion, after calculating a mean molar mass of the H_2O–CH_4 mixture. The molar volume at 22 °C was corrected for the volume change of the inclusion during cooling from the trapping conditions to room temperature using the equation of state of quartz, as described by Sterner and Bodnar (1991). The excess volumes were estimated using the PVT properties of the pure end member components H_2O (Haar et al., 1984) and CH_4 (Duan et al., 1992a). The results are listed in Table 2.

Molar volumes derived from our experimental data have been compared with those calculated using the thermodynamic model of Duan and Mao (2006). Results are listed in Table 4. Except for the results at 500 °C and 1000 bar, the differences in molar volume from the two studies are relatively small and the molar volumes determined in this study are generally larger than those predicted by the Duan and Mao (2006) thermodynamic model.

The difference in predicted molar volumes from the two studies increases with decreasing density (increasing molar volume). The largest differences in molar volume are for fluids trapped at 500 °C and 1000 bar and having homogenization temperatures >350 °C and densities <0.6 g/cm^3. It is not surprising that our experimentally-determined molar volumes might differ from those predicted by the thermodynamic model at these conditions because Duan and Mao (2006) state (p. 3374) that "*The optimal T–P range of this model for CH_4–H_2O system is 273–565 K [0–292 °C] and 1–2000 bar*". The discrepancy between the two data sets thus occurs in a temperature region that is at least 50 °C above the range in which the thermodynamic model is optimal.

It should also be noted that the Duan and Mao (2006) model is based only on data for solubility of CH_4 in H_2O and H_2O–salt solutions. Densities of the fluids are calculated, and some of the parameters used show large variations depending on the data source [i.e., the Henry's law coefficient at 500 K (227 °C – the highest temperature reported by Duan and Mao) varies by 13.3%, depending on which data source is used]. Moreover, only two studies, those of Sultanov et al. (1972) and Price (1979), present data above about 300 °C, and Duan and Mao (2006, page 3374) state that they did not use data from Sultanov et al. (1972) above 523 K (250 °C) or from Price (1979) above 565 K (292 K) in developing their model. Therefore, in developing their model, Duan and Mao (2006) did not include data in the temperature range of our measurements, and none of the lower temperature data they used were PVT data.

Zhang et al. (2007) have compared the slopes of isochores predicted by their thermodynamic model with our experimentally-derived iso-T_h lines. The two sets of data are in good agreement and Zhang et al. (2007) ascribed differences between the two studies to the volume discrepancy at homogenization. These differences are smaller for higher density fluids, and become larger with decreasing fluid density. In general, the differences for lower methane concentration fluids (0–3 mol.% CH_4) are smaller than for $\geqslant$4 mol.% CH_4 compositions.

4. SUMMARY

The synthetic fluid inclusion technique has been used to determine the PVTX properties of H_2O–CH_4 from the bubble point curve to 500 °C and 3 kbar for compositions $\leqslant$4 mol.% CH_4. Methane in the experiments was generated by the reaction of H_2O with aluminum carbide (Al_3C_4). Microthermometric data obtained from synthetic fluid inclusions trapped at 300–500 °C, 1–3 kbar and containing $\leqslant$4 mol.% CH_4 were used to determine the relationship between the slope of lines of constant homogenization temperature (iso-T_h lines) and homogenization temperature and composition. The slope ($\Delta P/\Delta T$) decreases systematically with increasing T_h for all compositions. At temperatures below about 300 °C the slopes of iso-T_h lines increase with increasing CH_4 concentration. The trend is reversed at higher temperatures. The slopes of iso-T_h lines were analyzed using a step-wise multiple regression technique to obtain an empirical relationship between the slope and the homogenization temperature and composition. The resulting algorithm is valid from the liquid–vapor boundary to 500 °C and 3 kbar for compositions $\leqslant$4 mol.% CH_4. Experimentally-derived volumetric data were compared with thermodynamics-based model results. The two sets

of data agree reasonably well for higher density fluids ($\rho > \sim 0.60$ g/cm^3), but significant discrepancies exist for lower density fluids (especially when $\rho < \sim 0.50$ g/cm^3).

ACKNOWLEDGMENTS

Mr. Charles Farley assisted with hydrothermal experiments and Raman analyses, and Dr. Jin Zhao assisted with X-ray diffraction analyses in the Crystallography Laboratory at Virginia Tech and provided the XRD pattern for corundum. Dr. Nizhou Han provided purified silica glass powder used in the experiments and Ms. Younan Chen from the Department of Statistics at Virginia Tech provided guidance on regression analysis of the data. Comments on an earlier version of this manuscript by Drs. P. Dove, F. Read, M. Schreiber and A. Sum are greatly appreciated, and review comments by J. Blencoe, I-Ming Chou, J. Dubessy, W. Lamb and Z. Duan significantly improved the interpretation and presentation. Funding for this research was provided by a grant from the U.S. Department of Energy [DE-FG05-89ER14065] and by NSF Grants EAR-0125918 and EAR-032219 to R.J.B.

REFERENCES

Adar F., Naudin C., Whitley A. and Bodnar R. J. (2004) Use of a microscope objective corrected for a cover glass to improve confocal spatial resolution inside a sample with finite index of refraction. *Appl. Spectrosc.* **58**(9), 1136–1137.

Ashmyan K. D., Skripka V. G. and Namiot Y. Y. (1985) The solubilities of methane and nitrogen in water at high temperatures and pressures. *Geokhimiya* **4**, 580–581.

Bodnar R. J. (1995) Experimental determination of the PVTX properties of aqueous solutions at elevated temperatures and pressures using synthetic fluid inclusions: H_2O–NaCl as an example. *J. Pure Appl. Chem.* **67**, 873–880.

Bodnar R. J. (2003a) Introduction to aqueous fluid systems. In Fluid Inclusions: Analysis and Interpretation (eds. I. Samson, A. Anderson, & D. Marshall). *Mineral. Assoc. Canada, Short Course* **32**, 81–99.

Bodnar R. J. (2003b) Reequilibration of fluid inclusions. In Fluid Inclusions: Analysis and Interpretation (eds. I. Samson, A. Anderson, & D. Marshall). *Mineral. Assoc. Canada, Short Course* **32**, 213-230.

Bodnar R. J., Binns P. R. and Hall D. L. (1989) Synthetic fluid inclusions. VI. Quantitative evaluation of the decrepitation behavior of fluid inclusions in quartz at one atmosphere confining pressure. *J. Metamorph. Geol.* **7**, 229–242.

Bodnar R. J. and Sterner S. M. (1985) Synthetic fluid inclusions in natural quartz. II. Application to PVT studies. *Geochim. Cosmochim. Acta* **49**, 1855–1859.

Bodnar R. J. and Sterner S. M. (1987) Synthetic fluid inclusions: Hydrothermal Experimental Techniques (eds. G.C. Ulmer and H.L. Barnes). Wiley-Interscience, New York, p. 423–457.

Bodnar R. J. and Vityk M. O. (1994) Interpretation of microthermometric data for H_2O–NaCl fluid inclusions. In *Fluids Inclusions in Minerals, Methods, Applications* (eds. B. De Vivo and M. L. Frezzotti). Virginia Tech, Blacksburg, VA, pp. 117–130.

Chou I.-M. (1986) Permeability of precious metals to hydrogen at 2 kb total pressure and elevated temperatures. *Am. J. Sci.* **286**, 638–658.

Chou I.-M., Sharma A., Burruss R. C., Hemley R., Goncharov A. F., Stern L. A. and Kirby S. H. (2001) Diamond-anvil cell observation of a new methane hydrate phase in the 100-MPa pressure range. *J. Phys. Chem. A* **105**, 4664–4668.

Chou I.-M., Song Y. and Burruss R. C. (2008) A new method for synthesizing fluid inclusions in fused silica capillaries containing organic and inorganic material. *Geochim. Cosmochim. Acta* **72**, 5217–5231.

Culberson O. L. and McKetta, Jr., J. J. (1951) Phase equilibria in hydrocarbon-water system. III. The solubility of methane in water at pressures to 10, 000 psi. *J. Petrol. Technol.* **4**, 223–226.

Duan Z. H. and Mao S. D. (2006) A thermodynamic model for calculating methane solubility, density and gas phase composition of methane-bearing aqueous fluids from 273 to 523 K and from 1 to 2000 bar. *Geochim. Cosmochim. Acta* **70**(13), 3369–3386.

Duan Z., Møller N. and Weare J. H. (1992a) An equation of state for the CH_4-CO_2–H_2O system. I. Pure systems from 0 to 1000 °C and from 0 to 8000 bar. *Geochim. Cosmochim. Acta* **56**, 2605–2617.

Duan Z., Møller N. and Weare J. H. (1992b) An equation of state for the CH_4–CO_2–H_2O system. II. Mixtures from 50 to 1000 °C and 0 to 1000 bar. *Geochim. Cosmochim. Acta* **56**, 2619–2631.

Duan Z., Møller N., Greenberg J. and Weare J. (1992c) The prediction of methane solubility in natural waters to high ionic strength from 0 to 250 °C and from 0 to 1600 bars. *Geochim. Cosmochim. Acta* **56**, 1451–1460.

Dubessy J., Buschaert S., Lamb W., Pironon J. and Thiéry R. (2001) Methane-bearing aqueous fluid inclusions: Raman analysis, thermodynamic modeling and application to petroleum basins. *Chem. Geol.* **173**, 193–205.

Guillaume D., Teinturier S., Dubessy J. and Pironon J. (2003) Calibration of methane analysis by Raman spectroscopy in H_2O–NaCl–CH_4 fluid inclusions. *Chem. Geol.* **194**, 41–49.

Haar L., Gallagher J. S. and Kell G. S. (1984) NBS/NBC steam tables. *Hemisphere*. p. 320.

Hall D. L. and Bodnar R. J. (1990) Methane in fluid inclusions from granulites: a product of hydrogen diffusion? *Geochim. Cosmochim. Acta* **54**, 641–651.

Hall D. L., Bodnar R. J. and Craig J. R. (1991) Evidence for postentrapment diffusion of hydrogen into peak metamorphic fluid inclusions from the massive sulfide deposits at Ducktown, Tennessee. *Am. Mineral.* **76**, 1344–1355.

Hanor J. S. (1980) Dissolved methane in sedimentary brines: potential effect on the PVT properties of fluid inclusions. *Econ. Geol.* **75**, 603–617.

Hao F., Li S., Sun Y. and Zhang Q. (1998) Geology, compositional heterogeneities, and geochemical origin of the Yacheng gas field, Qiongdongnan Basin, South China Sea. *AAPG Bull.* **82**, 1372–1384.

Invernizzi C., Vityk M. O., Cello G. and Bodnar R. J. (1998) Fluid inclusions in high pressure/low temperature rocks from the Calabrian Arc (southern Italy): the burial and exhumation history of the subduction-related Diamante–Terranova unit. *J. Metamorph. Geol.* **16**, 247–258.

Jacobs G. K. and Kerrick D. M. (1981) Methane: an equation of state with application to the ternary system H_2O–CO_2–CH_4. *Geochim. Cosmochim. Acta* **45**, 607–614.

Kelley D. S. (1996) Methane-bearing fluids in the oceanic crust: Gabbro-hosted fluid inclusions from the southwest Indian Ridge. *J. Geophys. Res.* **101**, 2943–2962.

Kisch H. J. and Van den Kerkhof A. M. (1991) CH_4-rich inclusions from quartz veins in the Valley- and Ridge province and the anthracite fields of the Pennsylvania Appalachians. *Am. Mineral.* **76**, 320–340.

Krader T. and Franck E. U. (1986) Phase equilibria and critical phenomena of the ternary system H_2O–CH_4–NaCl to 500 °C and 2500 bar. *Physica B+C* **139–140**, 66–69.

Lamb W. M., Popp R. K. and Boockoff L. A. (1996) The determination of phase relations in the CH_4–H_2O–NaCl system

at 1 kbar, 400–600 °C using synthetic fluid inclusions. *Geochim. Cosmochim. Acta* **60**, 1885–1897.

Lamb W. M., McShane C. J. and Popp R. K. (2002) Phase relations in the CH_4–H_2O–NaCl system at 2 kbar, 300–600 °C as determined using synthetic fluid inclusions. *Geochim. Cosmochim. Acta* **66**, 3971–3986.

Lemmon E. W., McLinden M. O. and Friend D. G. (2005) Thermophysical properties of fluid systems. In NIST Chemistry Web Book, NIST Standard Reference Database Number 69 (eds. P. J. Linstrom and W. G. Mallard). National Institute of Standards and Technology.

Lin F., Bodnar R. J. and Becker S. P. (2007) Experimental determination of the Raman CH_4 v1 band position from 1 to 650 bars and 0.3–22 °C: application to fluid inclusion studies. *Geochim. Cosmochim. Acta* **71**, 3746–3756.

Lu W., Chou I.-M., Burruss R. C. and Song Y. (2007) A unified equation for calculating methane vapor pressures in the CH_4–H_2O system with measured Raman shifts. *Geochim. Cosmochim. Acta* **71**, 3969–3978.

Mavrogenes J. A. and Bodnar R. J. (1994) Hydrogen movement into and out of fluid inclusions in quartz: experimental evidence and geologic implications. *Geochim. Cosmochim. Acta* **58**, 141–148.

Mullis J., Dubessy J., Poty B. and O'Neil J. (1994) Fluid regimes during late stages of a continental collision: physical, chemical, and stable isotope measurements of fluid inclusions in fissure quartz from a geotraverse through the Central Alps, Switzerland. *Geochim. Cosmochim. Acta* **58**, 2239–2267.

Murphy P. J. and Roberts S. (1997) Melting and nucleation behaviour of clathrates in multivolatile fluid inclusions: evidence of thermodynamic disequilibrium. *Chem. Geol.* **135**, 1–20.

Paglia G. (2004) Determination of the structure of γ-alumina using empirical and first principles calculations combined with supporting experiments. Ph.D. Thesis, Curtin University of Technology, Australia, p. 341.

Pironon J., Grimmer J. O. W., Teinturier S., Guillaume D. and Dubessy J. (2003) Dissolved methane in water: temperature effect on Raman quantification in fluid inclusions. *J. Geochem. Explor.* **78–79**, 111–115.

Price L. C. (1979) Aqueous solubility of methane at elevated pressures and temperatures. *AAPG Bull.* **63**, 1527–1533.

Roedder E. (1971) Metastability in fluid inclusions. *Soc. Mining Gel. Japan, Spec. Issue* **3**, 327–334.

Roedder E. (1984) Fluid inclusions. Reviews in Mineralogy, vol. 12. Mineralogical Society of America, p. 644p.

Roedder E. and Bodnar R. J. (1980) Geologic pressure determinations from fluid inclusion studies. *Annu. Rev. Earth Planet. Sci.* **8**, 263–301.

Rosso K. M. and Bodnar R. J. (1995) Detection limits of CO_2 in fluid inclusions using microthermometry and laser Raman spectroscopy and the spectroscopic characterization of CO_2. *Geochim. Cosmochim. Acta* **59**(19), 3961–3975.

Saxena S. K. and Fei Y. (1988) Fluid mixtures in the C–O–H system at high pressure and temperature. *Geochim. Cosmochim. Acta* **52**, 505–512.

Schmidt C. and Bodnar R. J. (2000) Synthetic fluid inclusions: XVI. PVTX properties in the system H_2O–NaCl–CO_2 at elevated temperatures, pressures, and salinities. *Geochim. Cosmochim. Acta* **64**, 3853–3869.

Schmidt C., Rosso K. M. and Bodnar R. J. (1995) Synthetic fluid inclusions. XIII: experimental determination of the PVTX properties in the system (H_2O + 40 wt.% NaCl) – CO_2 at elevated temperatures and pressures. *Geochim. Cosmochim. Acta* **59**, 3953–3959.

Shang L., Chou I., Lu W., Burruss R. C. and Zhang Y. (2009) Determination of diffusion coefficients of hydrogen in fused silica between 296 and 523 K by Raman spectroscopy and application of fused silica capillaries in studying redox reactions. *Geochim. Cosmochim. Acta* **73**, 5435–5443.

Sterner S. M. and Bodnar R. J. (1984) Synthetic fluid inclusions in natural quartz. I. Compositional types synthesized and applications to experimental geochemistry. *Geochim. Cosmochim. Acta* **48**, 2659–2668.

Sterner S. M. and Bodnar R. J. (1991) Synthetic fluid inclusions. X: Experimental determination of *P–V–T–X* properties in the CO_2–H_2O system to 6 kb and 700 °C. *Am. J. Sci.* **291**, 1–54.

Sultanov R. G., Skripka V. G. and Namoit A. Y. (1972) Phase equilibrium and critical effect of water–methane system under increased temperature and pressure. *Zhurnal Fizicheskoi khimi* **46**(8), 2160.

Vityk M. O., Bodnar R. J. and Dudok I. V. (1996) Hydrocarbon inclusions in Marmarosh Diamonds: evidence for tectonic history of the folded Carpathians? *Tectonophysics* **255**, 163–174.

Welsh H. (1973) Die Systeme Xenon-Wasser und Methan-Wasser bei hohen Drücken und Temperaturen. Ph.D. Thesis, Universität Karlsruhe, Karlsruhe, p. 41.

Wopenka B. and Pasteris J. D. (1987) Raman intensities and detection limits of geochemically relevant gas mixtures for a laser Raman microprobe. *Anal. Chem.* **59**, 2165–2170.

Zhang C., Duan Z. and Zhang Z. (2007) Molecular dynamics simulation of the CH4 and CH_4–H_2O systems up to 10 GPa and 273 K. *Geochim. Cosmochim. Acta* **71**, 2036–2055.

Zhang Y. and Frantz J. D. (1992) Hydrothermal reactions involving equilibrium between minerals and mixed volatiles. 2. Investigation of fluid properties in the CO_2-CH_4–H_2O system using synthetic fluid inclusions. *Chem. Geol.* **100**, 51–72.

Associate editor: Zhenhao Duan